The Astrophysical Journal, 592:L103–L106, 2003 August 1

HIGH-RESOLUTION BROADBAND SPECTROSCOPY USING AN EXTERNALLY DISPERSED INTERFEROMETER

David J. Erskine,[1] Jerry Edelstein,[2] W. Michael Feuerstein,[2] and Barry Welsh[2]
Received 2002 December 5; accepted 2003 June 24; published 2003 July 2

ABSTRACT

An externally dispersed interferometer (EDI) is a series combination of a fixed delay interferometer and an external grating spectrograph. We describe how the EDI can boost the effective resolving power of an echelle or linear grating spectrograph by a factor of 2–3 or more over the spectrograph's full bandwidth. The interferometer produces spectral fringes over the entire spectrograph's bandwidth. The fringes heterodyne with spectral features to provide a low spatial frequency moiré pattern. The heterodyning is numerically reversed to recover highly detailed spectral information unattainable by the spectrograph alone. We demonstrate resolution boosting for stellar and solar measurements of two-dimensional echelle and linear grating spectra. An effective spectral resolution of ∼100,000 has been obtained from the ∼50,000 resolution Lick Observatory two-dimensional echelle spectrograph, and that of ∼50,000 from an ∼20,000 resolution linear grating spectrograph.

Subject headings: instrumentation: interferometers — instrumentation: spectrographs — techniques: interferometric

1. INTRODUCTION

An externally dispersed interferometer (EDI) is a spectrograph hybrid of purely dispersive and interferometric systems recently developed for the precision measurement of Doppler radial velocities (Erskine & Ge 2000; Erskine 2002, 2003; Ge, Erskine, & Rushford 2002; Ge 2002). We describe a new application of the EDI: boosting the effective resolving power of a spectrograph by a factor of 2–3 over its full bandwidth. We have demonstrated resolution gain by adding an interferometer to both a linear grating spectrograph and an echelle spectrograph. EDI spectroscopy uses the same apparatus and raw data as used previously for EDI radial velocimetry measurements but applies a different data reduction procedure.

In EDI, fringes created by an external, unequal-arm white-light interferometer are imaged to a spectrograph's slit. The interferometer produces a transmission comb, sinusoidal in frequency ($\nu \equiv 1/\lambda$), over the entire bandwidth. This is analogous to the fiducial lines of an absorption cell, but with lines of exceedingly uniform spacing, shape, and amplitude over the entire bandwidth. The comb, in multiplication with the input spectrum, heterodynes fine spectral features into a low spatial frequency moiré pattern. The heterodyning is numerically reversed to recover highly detailed spectral information otherwise unattainable due to the spectrograph's resolution or detector Nyquist limits.

The EDI differs from previous hybrids (the Holographic Heterodyning Spectrograph and the Spatial Heterodyning Spectrograph) by using a dispersing element external to the interferometer rather than internal to it (Douglas 1997; Frandsen, Douglas, & Butcher 1993; Harlander, Reynolds, & Roesler 1992). Thus, the resulting EDI fringe spectral periodicity is uniform at all frequencies, allowing for a large operating bandwidth. In comparison with Fabry-Perot interferometer hybrids producing narrow spectral fiducials (Born & Wolf 1980, pp. 333–338; McMillan et al. 1993), the EDI's sinusoidal fiducial fringes transmit a greater average flux and offer a simple Fourier reduction of the heterodyning and an elegant trigonometric recovery of precise spectral information from as few as three phase-stepped data recordings.

2. APPARATUS

Details of the Lick EDI apparatus are shown in Erskine & Ge (2000), Ge et al. (2002), and Erskine (2002, 2003). Velocimetry data reduction and noise analysis are discussed in Erskine (2003). A wide-angle Michelson interferometer (Hilliard & Shepherd 1966) with unbalanced arms is used with a nonzero optical path length difference (delay, τ). Interferometer fringes created at the interferometer mirror plane are imaged to the spectrograph slit. Small delay changes ($\Delta\tau$) about a central delay value (τ_0) are described by an interferometer phase ($\phi = 2\pi\Delta\tau/\lambda$, where $\tau = \tau_0 + \Delta\tau$). Data can be taken in two modes in which ϕ is either uniform (uniphase) or varying (multiphase) spatially. In the latter, an interferometer mirror is tilted so that ϕ varies across the slit's length (Fig. 1*a*), and the full range of ϕ can be sampled in a single exposure. In the uniphase fringe mode, the interferometer mirrors are parallel, ϕ is constant over the slit, and a minimum of three phase-stepped exposures are acquired. The uniphase mode can be used with zero slit length (see Fig. 2), which permits EDI application to one-dimensional imaging or echelle spectroscopy in which the cross-dispersion dimension must be preserved for angular or order information. To facilitate fixed-pattern noise rejection, we typically acquire multiple phase-stepped exposures for both recordings modes.

Our Lick apparatus was designed to demonstrate resolution boosting and was not optimized for sensitivity—we discarded one of the interferometer arm outputs, a 50% loss. (A Mach-Zehnder interferometer can use both arms.) Sensitivity was also diminished by nonunity fringe visibility ($\gamma \sim 0.7$) because a fringe stabilization scheme was not used. Optical surface losses are estimated as ∼15%.

3. THEORY

The conventional (purely dispersive spectroscopy) detected signal versus frequency $B_{\rm ord}(\nu)$ is the convolution of the intrinsic

[1] Lawrence Livermore National Laboratory, Mail Stop L-479, Livermore, CA 94550; erskine1@llnl.gov.
[2] Space Sciences Laboratory, University of California at Berkeley, Grizzly Peak at Centennial Drive, Berkeley, CA 94720-3411; jerrye@ssl.berkeley.edu, michf@ssl.berkeley.edu, bwelsh@ssl.berkeley.edu.

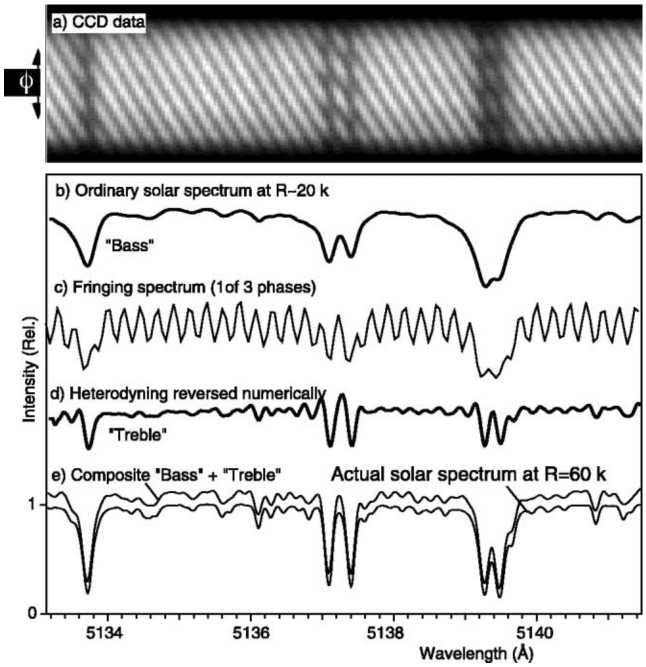

FIG. 1.—Demonstration of EDI 2.5 times resolution boosting for the solar spectrum using an $R \sim 20{,}000$ linear grating spectrograph and a $\tau = 1.1$ cm interferometer delay. (*a*) CCD recording of an EDI fringing spectrum in which ϕ varies transversely to dispersion (multiphase recording). (*b*) Ordinary spectrum $B_{\rm ord}(\lambda)$ derived from a histogram of (*a*). (*c*) Fringing spectrum phase exposure B_ϕ, from a lineout of (*a*), used to obtain (*d*), which is the fringing spectrum $B_{\rm edi}(\lambda)$. (*e*) EDI composite spectrum (*upper curve*), after equalization using iodine calibration spectra, which is nearly identical to a reference Kitt Peak FTS solar spectrum (*lower curve*) artificially blurred to $R = 60{,}000$. Data were taken 1998 June 16 at the Lawrence Livermore National Laboratory. Intensities are relative and have been offset.

input spectrum $S_0(\nu)$ and the spectroscope line-spread function LSF(ν),

$$B_{\rm ord}(\nu) = S_0(\nu) \otimes {\rm LSF}(\nu). \quad (1)$$

The FWHM of LSF(ν) is $\Delta\nu$ and is related to the resolution by $R = \nu/\Delta\nu$. The convolution of equation (1) expressed in Fourier space is

$$b_{\rm ord}(\rho) = s_0(\rho){\rm lsf}(\rho), \quad (2)$$

where the lower case symbols are the transformed versions and ρ is the spatial frequency along the dispersion axis in features per cm^{-1}. The lsf(ρ) is thus the transfer function of the impulse response LSF(ν). The normalized interferometer transmission $T'(\nu)$ is a sinusoidal spectral comb,

$$T'(\nu) = 1 + \gamma \cos(2\pi\tau\nu + \phi), \quad (3)$$

where γ is the interferometer visibility, assumed to be unity for now, and τ and ν are in units of cm and cm^{-1}, respectively. The spectra B_ϕ are recorded at multiple phases ϕ differing by ~90°, designated B_0, B_{90}, etc. (As few as three B_ϕ, ~120° apart, may be used.) Transmission through the interferometer multiplies $T'(\nu)$ with the spectrum *prior* to blurring by the external spectrograph. Hence, the EDI-detected signal is

$$B_{\rm edi}(\nu) = [S_0(\nu)T'(\nu)] \otimes {\rm LSF}(\nu). \quad (4)$$

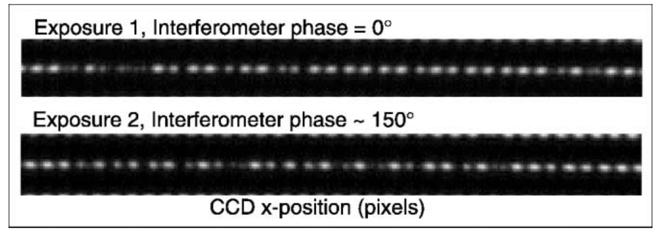

FIG. 2.—Subset of EDI echelle fringing raw spectra of the star ϵ Leo showing telluric lines near 6868 Å at two interferometer phases (ϕ), taken 2002 April using the Lick echelle spectrograph and a $\tau = 1.1$ cm delay. The change in the moiré pattern with ϕ indicates spectral features near periodicity $1/\tau = 0.9$ cm^{-1}.

Equation (4) is reexpressed as a sum of the ordinary spectrum plus two complex counterrotating fringing terms

$$B_{\rm edi}(\nu) = B_{\rm ord}(\nu) + \tfrac{1}{2}[S_0(\nu)e^{i\phi}e^{i2\pi\tau\nu} + S_0(\nu)e^{-i\phi}e^{-i2\pi\tau\nu}] \otimes {\rm LSF}(\nu). \quad (5)$$

High-resolution information is recovered by isolating a fringing component and reversing the heterodyning. The scalar spectrum is converted to a complex vector spectrum called a "whirl," $\boldsymbol{W}(\nu)$, by using a linear combination of the phased exposures B_ϕ that have been numerically rotated in synchrony with each exposure's phase-step value. The whirl for four-phase recording every 90° is

$$\boldsymbol{W}(\nu) = \tfrac{1}{4}(B_0 e^{i0^\circ} + B_{90}e^{i90^\circ} + B_{180}e^{i180^\circ} + B_{270}e^{i270^\circ}) \quad (6)$$

or

$$\boldsymbol{W}(\nu) = \tfrac{1}{4}[(B_0 - B_{180}) + i(B_{90} - B_{270})]. \quad (7)$$

Applying equation (6) or equation (7) to equation (5), we get

$$\boldsymbol{W}(\nu) = \tfrac{1}{2}[e^{i2\pi\tau\nu}S_0(\nu)] \otimes {\rm LSF}(\nu). \quad (8)$$

The Fourier transform of the whirl is then

$$\boldsymbol{w}(\rho) = \tfrac{1}{2}\gamma s_0(\rho + \tau){\rm lsf}(\rho), \quad (9)$$

where we include the interferometer visibility (γ) previously taken as unity. This important equation describes the EDI formation of moiré fringes, a heterodyning effect expressed in the $s_0(\rho + \tau)$ argument. Fine spectral details having high ρ are heterodyned (shifted by τ) to low ρ, prior to blurring by the spectrograph's line-spread function.

To obtain the EDI spectra, the optical heterodyning is numerically reversed, and the ordinary and fringing spectral components are combined. The latter is analogous to combining the "treble" and "bass" channels of an audio system to obtain a more full-bodied sound. The bass channel is the ordinary spectrum, and the treble channel is the fringing spectrum containing higher resolution information. The ordinary spectrum is determined by summing the phase-stepped data so that the fringing terms are canceled out,

$$B_{\rm ord}(\nu) = \tfrac{1}{4}(B_0 + B_{180} + B_{90} + B_{270}). \quad (10)$$

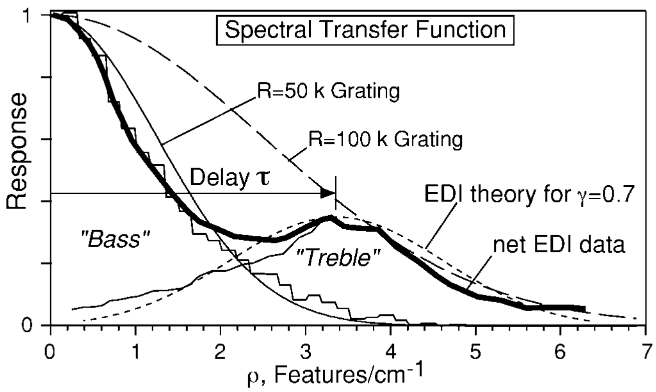

FIG. 3.—EDI spectral response functions $|b(\rho)/s_0(\rho)|$ for ordinary and fringing components as a function of spectral feature frequency ρ shown for theoretical and measured Lick echelle α Vir data. The theoretical ordinary spectrum response (*thin solid curve*) is modeled by a Gaussian lsf(ρ) centered at $\rho = 0$ with a width corresponding to an $R = 50{,}000$ grating. The EDI fringing spectrum response (*short-dashed curve*) is the ordinary response shifted by the $\tau \sim 3.3$ cm delay and scaled by $\gamma/2$, where the visibility $\gamma = 0.7$. The measured ordinary ("Bass") and fringing ("Treble") spectral responses are similar to their theoretical curves. The net EDI response $|b_{\rm net}(\rho)/s_0(\rho)|$ (*thick solid curve*), obtained from the quadrature combination of the ordinary and fringing terms, is enveloped by the theoretical $R = 100{,}000$ grating response (*long-dashed curve*) and, for high-resolution information at high ρ, follows this curve.

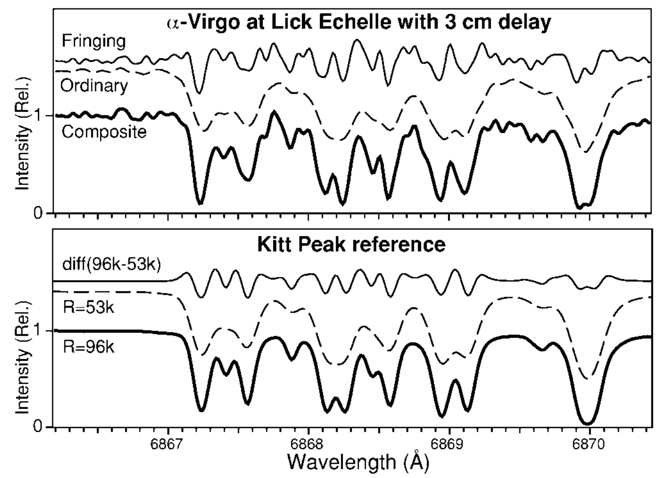

FIG. 4.—EDI spectral resolution boosting of ~2 times is demonstrated for oxygen telluric lines in the Lick $R = 50{,}000$ echelle spectrum of α Vir. *Top*: Measured EDI ordinary spectrum (*dashed line*) and fringing spectrum (*thin solid line*) combined to form the composite spectrum (*thick solid line*). The fringing spectrum provides high spatial frequency information that boosts the effective resolution. *Bottom*: Reference solar spectrum blurred to $R = 53{,}000$ (*dashed line*), $R = 96{,}000$ (*thick solid line*), and their difference (*thin solid line*) compared closely with the EDI spectral components and the composite. The curves are vertically offset. Data at the ends of the band were truncated in the analyses.

To recover high-frequency spectral components from the data, we Fourier transform $\boldsymbol{W}(\nu)$ to $\boldsymbol{w}(\rho)$, translate $\boldsymbol{w}(\rho)$ by τ, and scale it by $2/\gamma$. We then copy the positive frequency branch to the negative branch, after taking the complex conjugate, and form the EDI fringe "treble" frequency response $b'_{\rm edi}(\rho)$, shown in Figure 3 as the ($\rho = \tau$)–shifted response curve. The optimal delay value of $\tau \sim 1/\delta\nu = R/\nu$ will shift the heterodyned fringing response peak to the shoulder of the ordinary response peak. For example, $\tau = 1$ cm for an $R = 20{,}000$ grating at $\nu = 20{,}000$ cm^{-1} (5000 Å), and $\tau = 3$ cm for $R = 60{,}000$.

To obtain the net spectrum $B_{\rm net}(\nu)$, we form a weighted composite $b_{\rm net}(\rho)$ from the fringing "treble" and ordinary "bass" response signal:

$$b_{\rm net}(\rho) = \frac{\alpha(\rho) b_{\rm ord}(\rho) + \beta(\rho) b'_{\rm edi}(\rho)}{\alpha(\rho) + \beta(\rho)}. \qquad (11)$$

The factors α and β are chosen to avoid noise from spectral regions with insignificant signals. An optimal signal-to-noise ratio (S/N) occurs when α and β are proportional to the bass and treble response functions. Finally, the real spectrum $B_{\rm net}(\nu)$ is obtained from the inverse transform of $b_{\rm net}(\rho)$.

The inflection in the net spectral response function $b_{\rm net}(\rho)$ (Fig. 3, *thick solid curve*) indicates that EDI sensitivity differs with ρ. Response equalization, analogous to audio bass and treble equalization, removes the inflection and can shape the final profile [$\mathrm{LSF_{net}}(\nu)$] to a desirable Gaussian and eliminate ringing in the LSF. Calibration spectra establish the scaling for equalization. During equalization, both the signal and the noise per ρ are equally scaled.

4. EXPERIMENTAL DEMONSTRATIONS

Figure 1 demonstrates EDI resolution boosting on solar spectra using an $R = 20{,}000$ linear grating, $\tau = 1.1$ cm, and the multiphase fringe mode. The measured composite spectra $B_{\rm net}(\nu)$ compare closely with a very high resolution solar spectra from the Kitt Peak Fourier transform spectrometer (FTS) that has been artificially blurred to $R = 60{,}000$, demonstrating a resolution boost of ~2.5 times while using the original $R = 20{,}000$ slit width.

Figure 2 shows a portion of the EDI raw spectra of ϵ Leo using the Lick Observatory two-dimensional echelle grating spectrograph (Vogt 1987), a $\tau = 1.1$ cm interferometer, and the uniphase mode. The spectrum was recorded over the full echelle bandwidth (~4000–8000 Å), and only a tiny subset is shown. The change in the fringing moiré pattern due to a 150° phase step shows the presence of information near the $1/\tau = 0.9$ cm^{-1} interferometer periodicity.

EDI uniphase spectra of α Virginis (B1 III) were acquired using the Lick echelle spectrograph and $\tau \sim 3.3$ cm. Figure 4 shows a small subset of the EDI spectra about the oxygen telluric lines (~6868 Å) and Kitt Peak FTS solar reference spectra. The measured EDI ordinary spectrum, with $R \sim 53{,}000$ as limited by the echelle spectrograph, cannot resolve several split lines. The split line features are resolved by including the high-frequency features in the EDI fringing spectrum. The ~2 times EDI effective resolution gain is seen by comparing the reference solar spectrum, blurred to $R = 53{,}000$ and $R = 96{,}000$, with the ordinary and EDI composite spectra. The resolution gain occurs over the entire echelle bandwidth. The comparison of the telluric lines between starlight and sunlight is appropriate because both are subject to similar absorption by oxygen in the Earth's atmosphere.

Figure 3 shows the EDI and conventional Lick echelle instrument responses versus ρ. The $R = 50{,}000$ grating used alone is not sensitive to features with $\rho > 3$ cm. Introducing the interferometer shifts the grating response to $\rho = \tau = 3.3$ cm, where the $\rho > 3$ cm response is nearly equal to that of a model Gaussian $R = 100{,}000$ grating. Hence, for high ρ, where the important science information resides, the effective resolution has been boosted ~2 times. A boost of 2.5 times would theoretically occur for $\gamma = 1$ and $\tau = 3.6$ cm. A standard interferometer-fringe stabilization system would improve the observed $\gamma \sim 0.7$ to $\gamma \sim 0.95$.

4.1. *Sensitivity and Noise*

We briefly consider EDI sensitivity and noise, leaving a complete treatment to future publications. The EDI noise per spectral interval $\sigma_{B(\nu)\mathrm{net}}$ in the combined EDI spectra $B_{\mathrm{net}}(\nu)$ is determined by the noise in the ordinary B_{ord} and fringing B_{edi} spectral components. The noise for the ordinary component (see eq. [10]) is the same (in both ν- and ρ-space) as that for the conventional grating spectrograph for the same total exposure time because each phase-recording B_{ϕ} is an independent measurement.

The noise for the EDI and ordinary components are similar because the EDI component (eq. [6]) is constructed of the same B_{ϕ} terms as the ordinary component (eq. [10]), differing only by unity magnitude phasors. The phasors do not affect the net noise statistically because B_{ϕ} are independent and because the phasors only rotate B_{ϕ}. Random noise in $B(\nu)$ produces uniform random noise in $b(\rho)$. Hence, the same noise magnitude per ρ-bin exists for both $b_{\mathrm{ord}}(\rho)$ and $b'_{\mathrm{edi}}(\rho)$. Furthermore, the noise per ρ-bin in $b_{\mathrm{net}}(\rho)$ is almost the same as that for its components b_{ord} and b'_{edi} because the net response is formed from a weighted composite (eq. [11]) that effectively includes only one of the two components at each ρ. Hence, before equalization, $\sigma_{B(\nu)\mathrm{net}} \approx \sigma_{B(\nu)\mathrm{conv}} \approx \sigma_{B(\nu)\mathrm{edi}}$.

Equalization will affect noise in the final spectrum. The equalization process scales the noise per ρ-bin for only the mid-ρ region. Therefore, noise for high spectral resolution features (high ρ) is not affected. Noise for mid-ρ features will be scaled by a factor U, the ratio of equalized to unequalized responses (see Fig. 3) at the mid-ρ response notch. The value of U will depend on τ/R and γ and is ~2 here. For broad ($\rho < 1$ cm), midrange ($\rho \sim 2$ cm), and narrow ($\rho > 3$ cm) spectral feature sizes, for example, our EDI instrument's predicted net continuum-to-noise ratios (C/Ns) are ~80%, ~50%, and ~100% of the conventional C/N of an $R = 100{,}000$ grating, respectively. The C/N for the unequalized EDI net and conventional spectra is ~37 at 18 pixel Å^{-1}, or $\sigma_{B(\nu)\mathrm{conv}} \sim \sigma_{B(\nu)\mathrm{net}} \sim$ 3%. Our equalized net EDI spectrum (Fig. 4) noise is $\sigma_{B(\nu)\mathrm{equalized}} \sim 5\%$, or C/N ~ 20. This is consistent with the upper limit $\sigma_{B(\nu)\mathrm{equalized}} \leq U\sigma_{B(\nu)\mathrm{net}}$ found when the noise at all ρ is scaled by U.

4.2. *Multiple-Delay EDI*

Relative to grating spectrographs alone, the EDI is several times more compact per resolution and provides a more stable LSF for high spectral details. Further development of the EDI promises benefits to multiobject and slit imaging spectroscopy and to smaller and more economical high-resolution instruments. Versions of EDI having multiple delays can achieve higher resolution with a modest trade-off of photon noise. The EDI interferometer can be modified to simultaneously imprint a delay τ_m on M different paths through the same spectrograph and to detect these on separate regions of the detector. This forms a multiple-delay EDI that, if τ_m discretely covers ρ-space, yields a spectrograph with resolution boosting roughly proportional to $2M$. The photon S/N will decrease approximately proportional to $1/\sqrt{M}$ because the total flux is subdivided into M channels. For example, an $R = 20{,}000$ grating using a three-delay EDI having $\tau_m = 1$, 2, and 3 cm can attain a resolution boost of ~7 times. As $M \rightarrow \infty$, we approach the regime of an FTS that scans τ quasi-continuously in M exposures. In Figure 3, the FTS response function would have M very narrow peaks of $1/\sqrt{M}$ height distributed over the ρ-range of interest. Hence, the single-delay EDI photon S/N is better than that of the FTS by $\sim\sqrt{M} \sim [R(\mathrm{BW}/\lambda)]^{1/2} \sim 100$ for an $R = 20{,}000$, a bandwidth BW $= 4000$ Å, and average $\lambda = 6000$ Å (e.g., Beer 1992, p. 66).

Tim Erskine assisted in the data taking, and Shauna Sallmen helped with the echelle data reduction. We thank the Lick Observatory and staff for the use of their facility. Reference solar spectra were provided by Kitt Peak/NOAO. Work was supported by CalSpace/Lockheed, NASA grants NAG5-9091 and NAG5-3051, and was performed under auspices of the US DOE by the University of California, Lawrence Livermore National Laboratory contract W-7405-Eng-48.

REFERENCES

Beer, R. 1992, Remote Sensing by Fourier Transform Spectrometry (New York: Wiley)
Born, M., & Wolf, E. 1980, Principles of Optics (6th ed.; Oxford: Pergammon)
Douglas, N. 1997, PASP, 109, 151
Erskine, D. 2002, Combined Dispersive/Interference Spectroscopy for Producing a Vector Spectrum. US Patent Number 6,351,307, issued 2002 February 26
———. 2003, PASP, 115, 255
Erskine, D., & Ge, J. 2000, in ASP Conf. Ser. 195, Imaging the Universe in Three Dimensions: Astrophysics with Advanced Multi-Wavelength Imaging Devices, ed. W. van Breugel & J. Bland-Hawthorn (San Francisco: ASP), 501
Frandsen, S., Douglas, N., & Butcher, H. 1993, A&A, 279, 310
Ge, J. 2002, ApJ, 571, L165 (erratum, in press [2003])
Ge, J., Erskine, D., & Rushford, M. 2002, PASP, 114, 1016
Harlander, J., Reynolds, R. J., & Roesler, F. L. 1992, ApJ, 396, 730
Hilliard, R., & Shepherd, G. 1966, J. Opt. Soc. Am., 56, 362
McMillan, R., Moore, T., Perry, M., & Smith, P. 1993, ApJ, 403, 801
Vogt, S. S. 1987, PASP, 99, 1214